ACS APPLIED MATERIALS & INTERFACES

Research Article

www.acsami.org

An Alternative Approach to Evaluate the Wettability of Carbon Fiber Substrates

Pradeep Kumar Sow, Sebastian Prass, and Walter Mérida*

Clean Energy Research Centre, The University of British Columbia, 6250 Applied Science Lane, Vancouver, British Columbia, Canada V6T 1Z4

Supporting Information

ABSTRACT: The wettability of carbon fiber substrate plays an important role in a vast number of electrochemical energy production and storage technologies. Here, we report an alternative approach to evaluate the relative wettability for three substrates with the solid−liquid (S−L) interfacial area as the wettability parameter. We applied electrochemical techniques to quantify the S−L interfacial area and obtained the relative wettability on for three substrates with varying fiber morphology. This work proposes and validates a methodology to experimentally measure the substrate wettability and elucidates important aspects of the relevant wetting phenomena. Our results indicate that the wettability of carbon fiber substrate is affected by the liquid intrusion resulting from the instability of the Cassie−Baxter wetting state and that the contact angle is not dependent on the S−L interfacial area under the droplet. The present technique can be used to characterize the surface wettability of a wide range of conductive surfaces with irregular and multiscale surface roughness features.

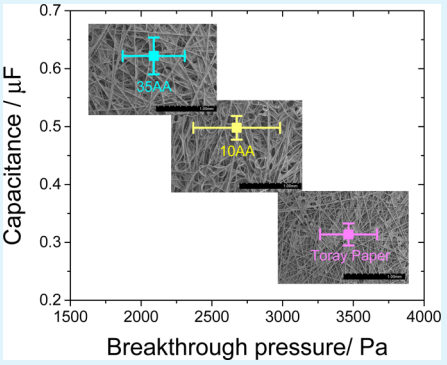

KEYWORDS: *carbon fiber, wettability, contact angle, double layer capacitance, gas diffusion layer*

1. INTRODUCTION

Due to their high thermal and electrical conductivity, porous carbon fiber substrates find application in a vast number of energy conversion and storage technologies including lithium-ion batteries,[1,2] lithium−air batteries,[3] redox-flow batteries,[4] fuel cells,[5] supercapacitors,[6,7] and so on. The surface wettability is one of the most important material properties for these applications because it can limit the overall device performance. A few illustrative examples are summarized in the following sections.

Carbon fiber substrates are widely used as gas diffusion layer (GDL) in hydrogen fuel cells. In this case, an increase in the substrate hydrophobicity enhances the fuel cell performance by facilitating water transport, especially during high current density operation.[8−13] In contrast to the hydrogen fuel cell, reduced anode hydrophobicity is desirable for direct methanol fuel cells in order to enhance the delivery and removal of the reactant and product, both of which are in aqueous phase.[14] Carbon fiber substrates are also widely used as the backing layer for supercapacitors, whose effective capacitance is a function of the ion accessible solid−liquid (S−L) interfacial area. One of the major objectives of the supercapacitor research is to increase the surface area of the substrate to enhance the capacitance. However, the translation of the available surface area to effective S−L interfacial area is dependent on the substrate hydrophobicity.[15−17] A higher capacitance can be obtained for hydrophilic substrates as compared to that of hydrophobic substrates featuring similar available surface area. Carbon fiber substrates are also used as the cathode material for the Li−air batteries, where higher wettability is desired to facilitate the ionic transfer during the charge and discharge processes.[3]

When a fixed volume of liquid is placed on the solid surface, the droplet attains a characteristic shape depending on the substrate wettability. Conventional evaluation of surface wettability utilizes one aspect of the droplet shape, which is the contact angle (CA) at the three-phase contact line. However, the limitations of the CA evaluation for rough surfaces (e.g., noncircularity of the three phase contact line, CA hysteresis, and lack of symmetry in the droplet shape[18−20]) are exacerbated for carbon fiber substrates, which has large roughness scales and anisotropic fiber distribution. The CA hysteresis provides a range of the possible CA values and shows significant overlap for carbon fiber substrates. The presence of the overlapping CA hysteresis ranges of different substrates complicates the evaluation of the relative wettability, and results in significant variation of the static CA.[21−25] The CA depends on the area near the three phase contact line which limits its ability to provide an accurate wettability information for rough surfaces.[26−28]

The limitations of the CA as the wettability parameter motivated our search for additional quantifiable parameters which are dependent on the substrate wettability. We selected the solid−liquid (S−L) interfacial area to quantify the relative

Received: July 30, 2015
Accepted: September 16, 2015
Published: September 16, 2015

DOI: 10.1021/acsami.5b06952
ACS Appl. Mater. Interfaces 2015, 7, 22029−22035

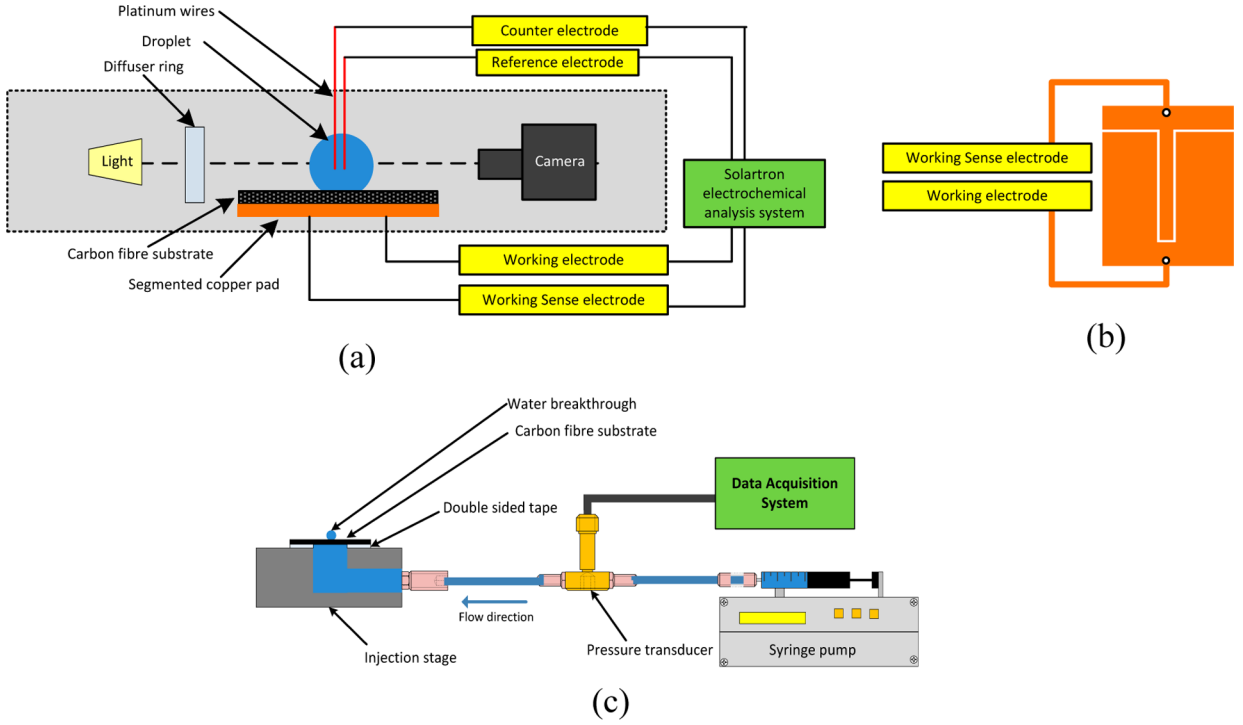

Figure 1. (a) Schematic diagram of the experimental setup used for the electrochemical and optical measurement of the substrate wettability. (b) Segmented contact pad on which the sample is placed. (c) Schematic diagram of the experimental setup for the breakthrough pressure measurements.

wettability. Our rationale for using the S−L interfacial area as a wetting parameter is that the wettability of any solid surface for a given liquid depends on the affinity of the liquid to form the S−L interface (which proceeds via minimization of the Gibbs free energy).[26] Hence, for a fixed droplet volume, the surface with higher hydrophobicity should have a lower S−L interfacial area. In this work, the wettability due to the S−L interfacial area was quantified by exploiting the ability of the carbon to support a stable double layer capacitor, which can be measured electrochemically. We have designed a methodology to evaluate the relative wettability of three commercially available carbon fiber substrates with similar order of CA values but varying (three-dimensional) fiber distributions. The differences in the wettability were found to depend on the intrusion of liquid into the fiber bulk arising from the instability of the Cassie−Baxter wetting state. The latter was evaluated using independent breakthrough pressure measurements.

The present method offers an alternative to the optical wettability measurement techniques, where the applicability of the CA evaluation process is limited. Our results establish the viability of the electrochemical method to evaluate wettability based on the S−L interfacial area under the droplet bulk, which is otherwise inaccessible using conventional visualization techniques.

2. EXPERIMENTAL SECTION

2.1. Materials. We studied three different commercially available carbon fiber materials: 10AA, 25AA (Ion-Power), Toray Paper/TGP-30 (fuel cell store). The liquid phase used in the wettability studies is an aqueous 0.1 M sodium sulfate (Fisher Scientific) solution, prepared in deionized water. All the measurements were conducted at room temperature (20 ± 2 °C) and 40−60% relative humidity.

2.2. Optical and Electrochemical Measurement Setup. Figure 1a shows a schematic diagram of the experimental setup used for optical and electrochemical analysis. The substrate was clamped on a sample holder consisting of segmented copper contact pads (Figure 1b). The segmentation of the contact pad enables separate current forcing and sensing electrodes, which removes the contact resistance between the contact pad and the sample. The bulk resistance of carbon fiber substrates are low (<15 mΩcm^2) ensuring negligible contribution of the substrate resistance in the evaluated values.[29] We used platinum microelectrodes (Fisher Scientific) with a thickness of 25 μm as counter and pseudoreference electrodes. The microelectrodes ensure minimum perturbation of the droplet shape, and the overall system can be identified as a miniaturized three-electrode electrochemical cell in which the liquid droplet acts as the electrolyte medium and the carbon fiber substrate as the working electrode. The experimental procedure involves gently placing the liquid droplet on the sample using a precision micropipette (Scilogex), followed by lowering the platinum wire assembly into the droplet bulk.

The distance between the platinum wires and the carbon fiber substrate was kept constant for all measurements and was monitored using a displacement sensor (Mitutoyo Corp.). The assembly was connected to an electrochemical analysis system (Solartron 1470E Cell Test System and a Solartron SI 1260 Impedance/Gain-Phase Analyzer) to facilitate the electrochemical measurement. The setup was coupled with a camera (Cannon EOS 1000D), lights and a diffuser ring to capture side view images of the droplet. The measurement of an apparent CA was done by analyzing the side view image (using open access software ImageJ) of a 10 μL droplet (0.1 M Na_2SO_4 solution in deionized water), placed on the substrate.

Electrochemical measurements were done using a droplet volume of 100 μL. The droplet placement was carried out by repeated feeding of the liquid to form a 100 μL droplet. The effect of the electrolyte (Na_2SO_4) concentration on the capacitance was evaluated in a range of 0.05−0.5 M, as shown in Supporting Information (Figure S1). The results show that the capacitances evaluated for different electrolyte concentrations are comparable within the error range. Further studies were carried out using 0.1 M Na_2SO_4 aqueous electrolyte solution. The added electrolyte imparts the necessary conductivity, and the high droplet volume ensures averaging of a larger surface area for consistent results. The CA evaluation was done using the electrolyte solution to maintain consistency with the electrochemical measurements.

DOI: 10.1021/acsami.5b06952
ACS Appl. Mater. Interfaces 2015, 7, 22029−22035

However, we also conducted the CA measurements using deionized water without any added electrolyte, and the contact angle values were found to be of similar order for both the cases.

2.3. Breakthrough Pressure Measurement Setup. Breakthrough pressure measurements were carried out by employing a bottom injection method.[21,30] Figure 1c shows the schematic diagram of the experimental setup. The experimental procedure involves placing a circular (5 mm) carbon fiber substrate on the injection stage made from polycarbonate sheet. The injection port diameter for the setup was 3.5 mm, which corresponds to the active area through which the intrusion occurs. The substrate was kept in place using a 3M double sided tape. The liquid is forced using a syringe pump (Harvard Apparatus, 11plus series syringe pump) while the pressure is measured using an Omega PX309 series pressure transducer at a sampling rate of 100 Hz.

3. RESULTS AND DISCUSSIONS

3.1. Contact Angle Evaluation. Figure 2a shows the SEM images of the carbon fiber substrates used in the present study

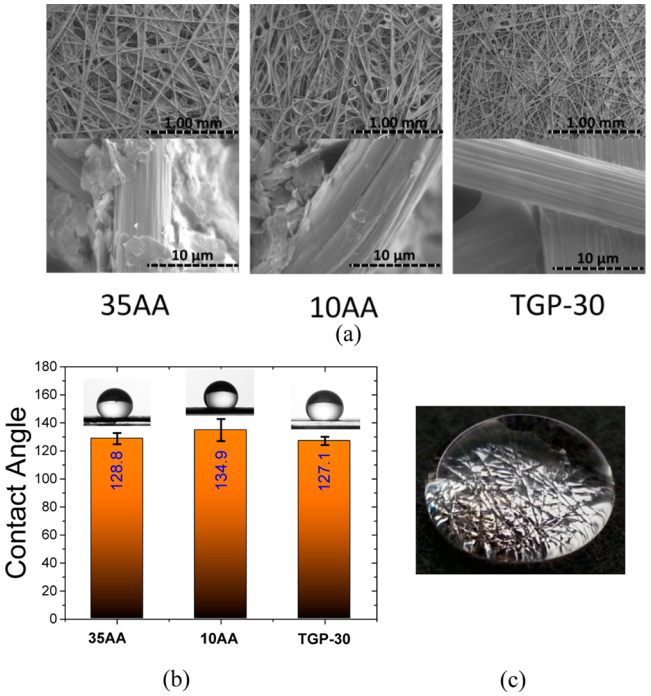

Figure 2. (a) SEM images of three carbon fiber substrates used in the present study. (b) Evaluated contact angle values for the three materials used in the present study. (c) An image of droplet on carbon fiber substrate (35AA) at a glancing angle, showing the droplet resting on the fractal structure from the carbon fibers.

at two different magnifications. The image shows the presence of three-dimensional fiber distributions and the roughness features on individual fibers. Statistical averages of the CA obtained for five samples of each material are shown in the Figure 2b along with the standard deviations in the form of error bars. The carbon fiber substrates showed pronounced hydrophobic behavior with CA values close to 130°, and the overall interaction can be classified as Cassie−Baxter wetting (CBW).[22] Similar orders of the static CA values have been reported in the literature for carbon fiber substrates,[11,21,31] and the high CA values are attributed to the heterogeneity of the interface under the droplet (Figure 2c). When a liquid droplet is placed on a solid surface, the droplet spreads until it attains the Gibbs free energy minimum, resulting in a unique droplet shape for a given surface wettability. For rough surfaces, multiple local Gibbs free energy minima exist, and hence, the droplet shape and the CA are dependent on the energy barrier separating these local energy minima.[26]

As the static CA values for the three samples are comparable within the error range, an estimation of relative wettability is difficult with the use of the optical measurement technique (Figure 2b). We address this limitation of the CA-based wettability evaluation with an electrochemical technique in the following section.

3.2. Electrochemical Assessment of the Substrate Wettability. We have utilized the ability of the carbon surface to support a stable double layer capacitor to quantify the wettability in terms of the S−L interfacial area. The double layer capacitance arising at the S−L interface is proportional to the S−L interfacial area[32,33] and the quantification can be carried out electrochemically (cyclic voltammetry, impedance spectroscopy, etc.). Recent efforts have been made to visualize the S−L interfacial area under the droplet for surfaces with patterned roughness features using environmental scanning electron microscopy,[34] X-rays,[35] confocal microscopy,[36] and so on. However, the applicability of the visualization techniques for the carbon fiber substrates is restricted by the limited optical accessibility and the irregular roughness features arising from the anisotropic fiber distribution.

In this work, electrochemical measurements (cyclic voltammetry and impedance spectroscopy) were conducted using the setup described in the Experimental Section with a droplet volume of 100 μL. The first step toward the evaluation process is to verify the presence of double layer capacitance. The validation was done by modeling the impedance spectra using a simplified equivalent circuit used for supercapacitor materials as shown in Figure 3a (inset).[37] The impedance spectra for all the materials were obtained in a frequency range of 100 kHz to 1 Hz with AC amplitude of 10 mV. To account for the nonideal capacitive properties of the double layer, we used a constant phase element (CPE) in lieu of an ideal capacitor in the equivalent circuit fitting, represented by equation[38]

$$-Z_{\text{imag}} = \frac{1}{Y_o}(j\omega)^{-n} \tag{1}$$

In the above relation, the CPE shows power law frequency dependence, where $-Z_{\text{imag}}$ corresponds to the imaginary component of the impedance, Y_o is the admittance and ω is the angular frequency. Depending on the value of n, the CPE can behave as a resistor ($n = 0$), inductor ($n = -1$), or a capacitor ($n = 1$).

For all the samples, the value of n was found to be ~0.98, along with high leakage resistance (R_L approximately 10^6−10^7 Ω), which supports the presence of stable double layer capacitance.

The cyclic voltammetry curves for all the samples showed a shape typically observed for the double layer capacitance. The quantification of the double layer capacitance is done by CV measurements, where the capacitance is evaluated using the relation

$$C = \frac{1}{2\upsilon(V_f - V_0)} \int_{V_0}^{V_f} I(V)dV \tag{2}$$

In the above equation, the integral term is evaluated as the area enclosed by the CV curve, υ represents the scan rate and $(V_f - V_0)$ represents the potential window. For the present analysis, a

DOI: 10.1021/acsami.5b06952
ACS Appl. Mater. Interfaces 2015, 7, 22029−22035

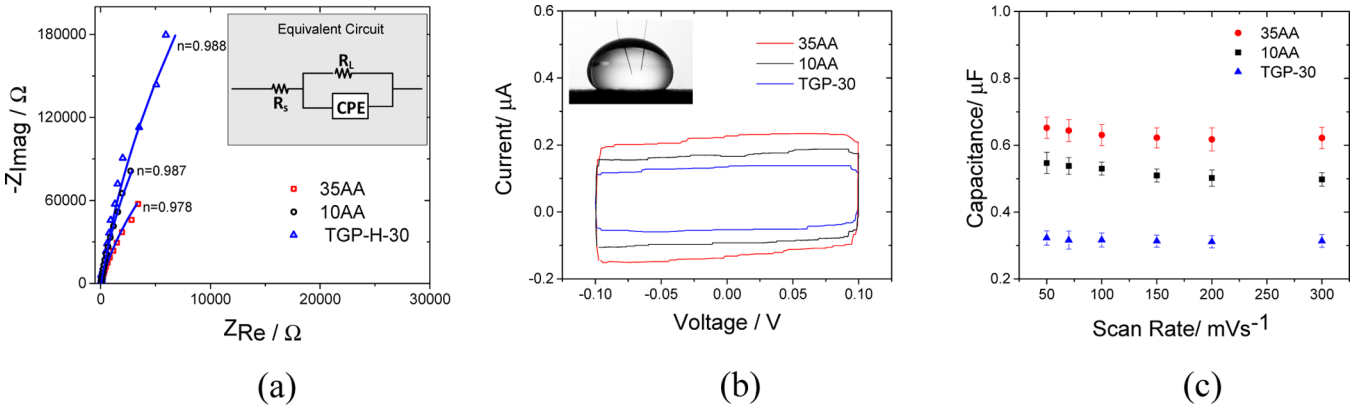

Figure 3. (a) Impedance spectra represented in the form of the Nyquist plot and (inset) the equivalent circuit used for fitting the impedance spectra. (b) Cyclic voltammetry curve for three different carbon fiber substrates at a scan rate of 300 mV/s and (inset) the side-view image of the droplet. (c) Capacitance of three different carbon fiber substrates with varying scan rates (50−300 mV/s).

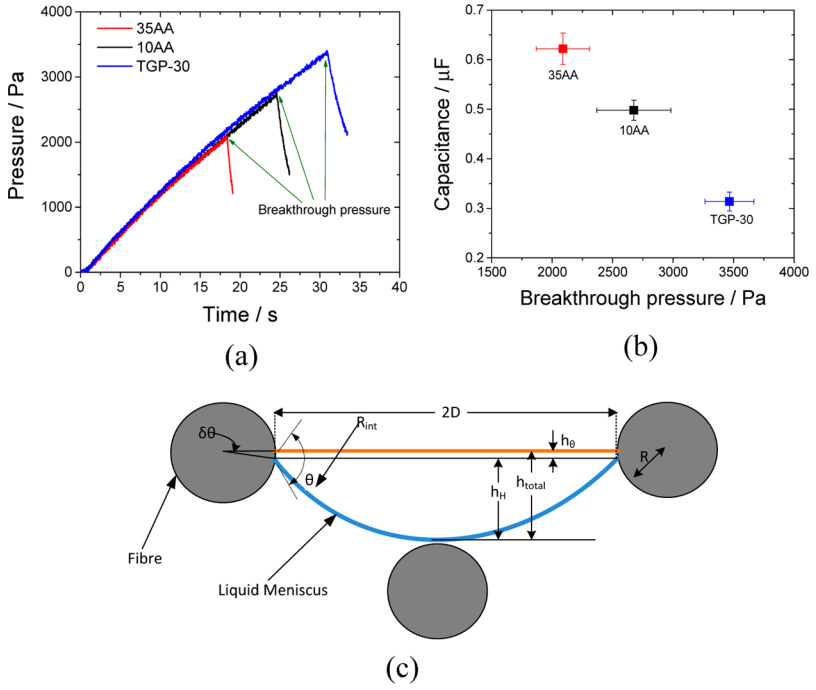

Figure 4. (a) Evolution of breakthrough pressure for different carbon fiber materials showing a linear increase in pressure with time for all the samples. (b) Plot of breakthrough pressure and capacitance for different samples. Values represent the average of five samples, and the error bars represent the standard deviation. (c) A simplified cross-sectional representation of the intrusion of the liquid meniscus between two cylindrical fibers.

potential window of 0.2 V (−0.1 to 0.1 V w.r.t. platinum pseudo reference electrode) was chosen and the evaluation was done for scan rates varying from 50 to 300 mV·s^{-1}. Figure 3b shows the cyclic voltammetry curves obtained for three materials. The capacitance values for these three materials are shown in Figure 3c. The capacitance was found to decrease (3−10%) with increase in the scan rate from 50 to 300 mV s^{-1}, which is attributed to the increasing diffusional resistance. The statistical average of the measured values is reported for five samples at each scan rate along with the standard deviation as the error bars. The error range was found to be small compared to the measured values. The capacitance was found to be distinct for all carbon fiber substrates within the error range (Figure 3c) and the order of capacitance is obtained as 35AA > 10AA > TGP-30. Because the capacitance is proportional to the S−L interfacial area, the surface with the lowest capacitance is the most hydrophobic, which, for the present case, is TGP-30. From the experimental results, the capacitance (and hence the S−L interfacial area) shows variation, while the CA values are of similar order for three substrates used in the present study.

Understanding the phenomenon governing the wettability of the carbon fiber substrate is fundamental toward tailoring the substrate property for specific applications. For a rough surface with multiscale roughness features, the overall wettability arises from the combined effect of the microscale roughness (fiber surface) and the macro-scale roughness (fiber distribution). Because the individual fibers have similar surface structures and diameters (7−14 μm), it can be concluded that the observed difference in the relative wettability is from the fiber distribution in three dimensions.

The projected diameter and the CA values (measured from the side-view image of the droplet) for a 100 μL droplet is of similar order (∼5 mm and ∼130°) for 35AA and TGP-30, while the capacitance of the 35AA (∼0.65 μF) was found to be

DOI: 10.1021/acsami.5b06952
ACS Appl. Mater. Interfaces 2015, 7, 22029−22035

twice as compared to the TGP-30 (~0.3 μF). We hypothesize that the variation in the measured capacitance (and hence the wettability) is affected by the degree of liquid intrusion into the fiber structure, which has been investigated experimentally in the following sections.

3.3. Breakthrough Pressure and Liquid Intrusion. To support our hypothesis, we measured the pressure required to force the liquid into the fiber matrix as potential metric to estimate of relative dominance of intrusion and the robustness of the Cassie−Baxter wetting state for the substrate.[39]

The pressure drop increased linearly with time with a sudden drop once the droplet emerged on the opposite side of the layer, which corresponds to the breakthrough pressure (Figure 4a). The flow rate used in the present study was 0.0017 mLs^{-1}. The highest breakthrough pressure was obtained for TGP-30 (~3500 Pa), while the lowest breakthrough pressure was obtained for 35AA (~2000 Pa). The order of the breakthrough pressure values for the three material was obtained as TGP-30 > 10AA > 35AA. The measurement was carried out for five samples of each material, and the average values are reported along with the error bars (standard deviation for five measurements) in order to obtain a statistical average and incorporate the variation in the material property. A comparison of the capacitance and the breakthrough pressure (Figure 4b) indicates an inverse relationship and the substrate with the highest breakthrough pressure demonstrates the lowest capacitance. From the data, we conclude that the enhanced wettability of the 35AA arises from the higher degree of intrusion resulting in the higher S−L interfacial area as compared to TGP-30 and 10AA. The pressure measurement serves as an independent verification for the proposed hypothesis and suggests that the intrusion of liquid affects the observed wettability of carbon fiber substrates.

With reference to wetting states, the intrusion of liquid into a roughness feature is a transitional intermediate between the Cassie−Baxter state and the Wenzel wetting state (complete intrusion). When a droplet is placed on the substrate, the transition can occur via two mechanisms: contact line sliding along the solid surface or the sagging of liquid meniscus while the three phase contact line stays pinned.[39−41] A simplified representation in two dimensions for the bending of the liquid meniscus between two fibers is shown in Figure 4c. The total intrusion depth (h_{total}) can be represented as the sum of the intrusion from sliding mechanism (h_θ) and from the sagging mechanism (h_H). The total intrusion depth can be evaluated based on the geometric constraints, as reported by Tuteja et al.:[39]

$$h_{total} = h_\theta + h_H = \frac{RD\sin\theta}{R_{int}} + \frac{D^2}{2R_{int}} \quad (3)$$

In the above equation, D represents the separation between the fibers, R is the radius of the fiber, and θ represents the equilibrium contact angle. For a fixed droplet volume, R_{int} is constant and represents the radius of curvature for the liquid meniscus trapped within the fiber arising from the balance of the body forces (gravity) to that of the Laplace pressure. For the liquid meniscus to come in contact with the next fiber layer, the necessary condition is that the total intrusion depth (h_{total}) should be higher than the fiber diameter ($2R$). The separation between the fibers ($2D$) on the top surface of the substrate is significantly higher than the fiber diameter ($2R$). Hence, the sagging mechanism (h_H) dominates the intrusion process as the contribution of h_θ is low (for $D \gg R \rightarrow h_H \gg h_\theta$). On the basis of the above discussion, for the same droplet volume, the total intrusion height (h_{total}) should be higher for the substrate with higher separation between the fibers ($2D$). From the SEM images (Figure 2a), the 35AA has lower surface fiber density as compared to the Toray paper (TGP-30) which explains the higher breakthrough pressure and the lower capacitance of the TGP-30 sample. With each intrusion step, the Laplace pressure resisting the intrusion increases and the process continues until it becomes equal to the pressure arising from the droplet weight. For a three-dimensional fiber structure, the length of the individual fiber is significantly higher than the fiber separation and there exists variation in the relative distance between the fibers along the fiber length. The fiber distribution affects the overall liquid meniscus shape as it can be seen in the glancing angle image of the droplet resting on the fiber structure (Figure 2c).

Our work illustrates that the CA values are not dependent on the S−L interfacial area, and this deduction is supported by previous works.[27,28] Hence, care should be taken while reporting the CA as a wettability parameter for carbon fiber substrates. On the basis of the present work, the wettability of a rough substrate should be treated in a three-dimensional domain, and the extent of intrusion should be incorporated into the overall wetting features. Moreover, the robust technique presented here can be adapted to the characterization and quality control of carbon fiber substrates during manufacturing processes. The technique provides a single parameter (capacitance) that encompasses several interlinked surface properties of the substrate, which includes the fiber structure, fiber distribution, surface wettability, and the degree of liquid intrusion.

4. CONCLUSIONS

In this work, we have demonstrated S−L interfacial area dependent wettability determination, where the quantification has been carried out using an electrochemical technique for carbon fiber substrates. It was found that the wettability of carbon fiber substrates is dependent on the degree of intrusion into the fiber matrix while the CA values were found to be independent of the S−L interfacial area. This work can be extended to study and characterize a wide range of rough conductive surfaces irrespective of the regularity of the roughness features and can augment our understanding of the wetting phenomenon on rough surfaces.

■ ASSOCIATED CONTENT

Supporting Information

The Supporting Information is available free of charge on the ACS Publications website at DOI: 10.1021/acsami.5b06952.

effect of electrolyte concentration (0.05, 0.1, and 0.5 M Na_2SO_4) on evaluated capacitance for 10AA GDL sample. (PDF)

■ AUTHOR INFORMATION

Corresponding Author

*E-mail: walter.merida@ubc.ca. Tel: 604-822-4189. Fax: 604-822-2403.

Author Contributions

The manuscript was written through contributions of all authors. All authors have given approval to the final version of the manuscript.

DOI: 10.1021/acsami.5b06952
ACS Appl. Mater. Interfaces 2015, 7, 22029−22035

Notes

The authors declare no competing financial interest.

■ ACKNOWLEDGMENTS

We thank Victor Lu for his help during the experiments. The authors acknowledge the Natural Sciences and Engineering Research Council of Canada (NSERC Grant Number: NSERC RGPIN 261625-13), and the Fraunhofer- UBC Clean Energy Partnership for the support of this research. SEM was performed at the Centre for High-Throughput Phenogenomics at the University of British Columbia, a facility supported by the Canada Foundation for Innovation, the British Columbia Knowledge Development Foundation, and the UBC Faculty of Dentistry. We extend our gratitude towards our lab members for the helpful discussions during the preparation of the manuscript.

■ REFERENCES

(1) Jung, H.-G.; Hassoun, J.; Park, J.-B.; Sun, Y.-K.; Scrosati, B. An Improved High-Performance Lithium-Air Battery. *Nat. Chem.* **2012**, *4*, 579−585.
(2) Wolf, H.; Pajkic, Z.; Gerdes, T.; Willert-Porada, M. Carbon−Fiber−Silicon-Nanocomposites for Lithium-Ion Battery Anodes by Microwave Plasma Chemical Vapor Deposition. *J. Power Sources* **2009**, *190*, 157−161.
(3) Zhang, J.; Ma, Z.; Yuan, X.; Li, L.; Ma, Z.-F.; Wilkinson, D. P.; Zhang, L. A Review of Cathode Materials and Structures for Rechargeable Lithium-Air Batteries. *Energy Environ. Sci.* **2015**, *8*, 2144−2198.
(4) Luo, X.; Lu, Z.; Xi, J.; Wu, Z.; Zhu, W.; Chen, L.; Qiu, X. Influences of Permeation of Vanadium Ions through PVDF-g-PSSA Membranes on Performances of Vanadium Redox Flow Batteries. *J. Phys. Chem. B* **2005**, *109*, 20310−20314.
(5) Cindrella, L.; Kannan, a. M.; Lin, J. F.; Saminathan, K.; Ho, Y.; Lin, C. W.; Wertz, J. Gas Diffusion Layer for Proton Exchange Membrane Fuel Cells—A review. *J. Power Sources* **2009**, *194*, 146−160.
(6) Pandey, G. P.; Rastogi, a. C.; Westgate, C. R. All-Solid-State Supercapacitors with Poly(3,4-ethylenedioxythiophene)-coated Carbon Fiber Paper Electrodes and Ionic Liquid Gel Polymer Electrolyte. *J. Power Sources* **2014**, *245*, 857−865.
(7) Algharaibeh, Z.; Liu, X.; Pickup, P. G. An Asymmetric Anthraquinone-modified Carbon/Ruthenium Oxide Supercapacitor. *J. Power Sources* **2009**, *187*, 640−643.
(8) Chou, Y.-I.; Siao, Z.-Y.; Chen, Y.-F.; Sung, L.-Y.; Yang, W.-M.; Wang, C.-C. Water Permeation Analysis on Gas Diffusion Layers of Proton Exchange Membrane Fuel Cells for Teflon-coating Annotation. *J. Power Sources* **2010**, *195*, 536−540.
(9) Li, H.; Tang, Y.; Wang, Z.; Shi, Z.; Wu, S.; Song, D.; Zhang, J.; Fatih, K.; Zhang, J.; Wang, H.; Liu, Z.; Abouatallah, R.; Mazza, A. A Review of Water Flooding Issues in the Proton Exchange Membrane Fuel Cell. *J. Power Sources* **2008**, *178*, 103−117.
(10) Mukherjee, P. P.; Kang, Q.; Wang, C.-Y. Pore-scale Modeling of Two-phase Transport in Polymer Electrolyte Fuel Cells—Progress and Perspective. *Energy Environ. Sci.* **2011**, *4*, 346−369.
(11) Thomas, Y. R. J.; Benayad, A.; Schroder, M.; Morin, A.; Pauchet, J. New Method for Super Hydrophobic Treatment of Gas Diffusion Layers for Proton Exchange Membrane Fuel Cells Using Electrochemical Reduction of Diazonium Salts. *ACS Appl. Mater. Interfaces* **2015**, *7* (27), 15068−15077.
(12) Ko, T.-J.; Kim, S. H.; Hong, B. K.; Lee, K.-R.; Oh, K. H.; Moon, M.-W. High Performance Gas Diffusion Layer with Hydrophobic Nanolayer under a Supersaturated Operation Condition for Fuel Cells. *ACS Appl. Mater. Interfaces* **2015**, *7*, 5506−5513.
(13) Friess, B. R.; Hoorfar, M. Measurement of Internal Wettability of Gas Diffusion Porous Media of Proton Exchange Membrane Fuel Cells. *J. Power Sources* **2010**, *195*, 4736−4742.
(14) Zhang, J.; Yin, G.-P.; Lai, Q.-Z.; Wang, Z.-B.; Cai, K.-D.; Liu, P. The Influence of Anode Gas Diffusion Layer on the Performance of Low-Temperature DMFC. *J. Power Sources* **2007**, *168*, 453−458.
(15) Cheng, Q.; Tang, J.; Ma, J.; Zhang, H.; Shinya, N.; Qin, L. C. Polyaniline-coated electro-etched Carbon Fiber Cloth Electrodes for Supercapacitors. *J. Phys. Chem. C* **2011**, *115*, 23584−23590.
(16) Hall, P. J.; Mirzaeian, M.; Fletcher, S. I.; Sillars, F. B.; Rennie, A. J. R.; Shitta-Bey, G. O.; Wilson, G.; Cruden, A.; Carter, R. Energy Storage in Electrochemical Capacitors: Designing Functional Materials to Improve Performance. *Energy Environ. Sci.* **2010**, *3*, 1238−1251.
(17) Sevilla, M.; Mokaya, R. Energy Storage Applications of Activated Carbons: Supercapacitors and Hydrogen Storage. *Energy Environ. Sci.* **2014**, *7*, 1250−1280.
(18) Dorrer, C.; Rühe, J. Contact Line Shape on Ultrahydrophobic Post Surfaces. *Langmuir* **2007**, *23*, 3179−3183.
(19) Srinivasan, S.; McKinley, G. H.; Cohen, R. E. Assessing the Accuracy of Contact Angle Measurements for Sessile Drops on Liquid-Repellent Surfaces. *Langmuir* **2011**, *27*, 13582−13589.
(20) Yeh, K. Y.; Chen, L. J.; Chang, J. Y. Contact Angle Hysteresis on Regular Pillar-like Hydrophobic Surfaces. *Langmuir* **2008**, *24*, 245−251.
(21) Santamaria, D.; Das, P. K.; MacDonald, J. C.; Weber, a. Z. Liquid-Water Interactions with Gas-Diffusion-Layer Surfaces. *J. Electrochem. Soc.* **2014**, *161*, F1184−F1193.
(22) Gauthier, E.; Hellstern, T.; Kevrekidis, I. G.; Benziger, J. Drop Detachment and Motion on Fuel Cell Electrode Materials. *ACS Appl. Mater. Interfaces* **2012**, *4*, 761−771.
(23) Kumbur, E. C.; Sharp, K. V.; Mench, M. M. Liquid Droplet Behavior and Instability in a Polymer Electrolyte Fuel Cell Flow Channel. *J. Power Sources* **2006**, *161*, 333−345.
(24) Das, P. K.; Grippin, A.; Kwong, A.; Weber, A. Z. Liquid-Water-Droplet Adhesion-Force Measurements on Fresh and Aged Fuel-Cell Gas-Diffusion Layers. *J. Electrochem. Soc.* **2012**, *159* (5), B489−B496.
(25) Cheung, P.; Fairweather, J. D.; Schwartz, D. T. Characterization of Internal Wetting in Polymer Electrolyte Membrane Gas Diffusion Layers. *J. Power Sources* **2009**, *187*, 487−492.
(26) Marmur, A. Soft Contact: Measurement and Interpretation of Contact Angles. *Soft Matter* **2006**, *2*, 12−17.
(27) Gao, L.; McCarthy, T. J. How Wenzel and Cassie Were Wrong. *Langmuir* **2007**, *23*, 3762−3765.
(28) Extrand, C. W.; Moon, S. I. Which Controls Wetting? Contact Line Versus Interfacial Area: Simple Experiments on Capillary Rise. *Langmuir* **2012**, *28*, 15629−15633.
(29) Sow, P. K.; Prass, S.; Kalisvaart, P.; Mérida, W. Deconvolution of Electrical Contact and Bulk Resistance of Gas Diffusion Layers for Fuel Cell Applications. *Int. J. Hydrogen Energy* **2015**, *40*, 2850−2861.
(30) Bazylak, A.; Sinton, D.; Djilali, N. Dynamic Water Transport and Droplet Emergence in PEMFC Gas Diffusion Layers. *J. Power Sources* **2008**, *176*, 240−246.
(31) Mortazavi, M.; Tajiri, K. Liquid Water Breakthrough Pressure Through Gas Diffusion Layer of Proton Exchange Membrane Fuel Cell. *Int. J. Hydrogen Energy* **2014**, *39*, 9409−9419.
(32) Zhang, L. L.; Zhao, X. S. Carbon-based Materials as Supercapacitor Electrodes. *Chem. Soc. Rev.* **2009**, *38*, 2520−2531.
(33) Frackowiak, E. Carbon Materials for Supercapacitor Application. *Phys. Chem. Chem. Phys.* **2007**, *9*, 1774−1785.
(34) Paxson, A. T.; Varanasi, K. K. Self-similarity of Contact Line Depinning from Textured Surfaces. *Nat. Commun.* **2013**, *4*, 1492.
(35) Antonini, C.; Lee, J. B.; Maitra, T.; Irvine, S.; Derome, D.; Tiwari, M. K.; Carmeliet, J.; Poulikakos, D. Unraveling Wetting Transition Through Surface Textures With X-rays: Liquid Meniscus Penetration Phenomena. *Sci. Rep.* **2014**, *4*, 4055.
(36) Papadopoulos, P.; Mammen, L.; Deng, X.; Vollmer, D.; Butt, H. How Superhydrophobicity Breaks Down. *Proc. Natl. Acad. Sci. U. S. A.* **2013**, *110*, 3254−3258.
(37) Frackowiak, E.; Béguin, F. Carbon Materials for the Electrochemical Storage of Energy in Capacitors. *Carbon* **2001**, *39*, 937−950.
(38) Sow, P. K.; Parvatalu, D.; Bhardwaj, A.; Prabhu, B. N.; Bhaskarwar, a. N.; Shukla, A. Impedance Spectroscopic Determination

DOI: 10.1021/acsami.5b06952
ACS Appl. Mater. Interfaces 2015, 7, 22029−22035

of Effect of Temperature on the Transport Resistances of an Electrodialysis Cell used for Concentration of Hydriodic Acid. *J. Appl. Electrochem.* **2013**, *43*, 31−41.
(39) Tuteja, A.; Choi, W.; Mabry, J. M.; McKinley, G. H.; Cohen, R. E. Robust Omniphobic Surfaces. *Proc. Natl. Acad. Sci. U. S. A.* **2008**, *105*, 18200−18205.
(40) Berthier, J.; Loe-Mie, F.; Tran, V. M.; Schoumacker, S.; Mittler, F.; Marchand, G.; Sarrut, N. On the Pinning of Interfaces on Micropillar Edges. *J. Colloid Interface Sci.* **2009**, *338*, 296−303.
(41) Wang, Z.; Wu, T. Modeling Pressure Stability and Contact-Angle Hysteresis of Superlyophobic Surfaces Based on Local Contact Line. *J. Phys. Chem. C* **2015**, *119* (23), 12916−12922.

DOI: 10.1021/acsami.5b06952
ACS Appl. Mater. Interfaces 2015, 7, 22029−22035